bond N–H(1)···O(1) (Table 6) also seems to exist in the present molecule. N, H(1), O(1), C′ and C^{α} are nearly coplanar with deviations less than 0·08 Å. From the hydrogen-bond distances and angles involving N, H(1), O(1) and *W*(2) (Table 6) it may be concluded that there is a bifurcated hydrogen bond. All pertinent intermolecular distances were examined. Apart from the hydrogen bonds, no contact appears to be incompatible with accepted van der Waals radii.

We thank the Council of Scientific and Industrial Research, India, for financial assistance.

References

ABRAHAM, R. J. & MCLAUCHLAN, K. A. (1962). *Mol. Phys.* **5**, 513–523.
ASHIDA, T. & KAKUDO, M. (1974). *Bull. Chem. Soc. Japan*, **47**, 1129–1133.
BENEDETTI, E., CIAJOLO, M. R. & MAISTO, A. (1974). *Acta Cryst.* B**30**, 1783–1788.
CROMER, D. T. & WABER, J. T. (1965). *Acta Cryst.* **18**, 104–109.
DONOHUE, J. & TRUEBLOOD, K. N. (1952). *Acta Cryst.* **5**, 419–413.
GERMAIN, G., MAIN, P. & WOOLFSON, M. M. (1971). *Acta Cryst.* A**27**, 368–376.
IUPAC–IUB COMMISSION ON BIOCHEMICAL NOMENCLATURE (1970). *J. Mol. Biol.* **52**, 1–17.
KARLE, I. L. (1970). *Acta Cryst.* B**26**, 765–770.
KOETZLE, T. F., LEHMANN, M. S. & HAMILTON, W. C. (1973). *Acta Cryst.* B**29**, 231–236.
PHILLIPS, D. C. (1954). *Acta Cryst.* **7**, 746–751.
RAMACHANDRAN, G. N., LAKSHMINARAYANAN, A .V., BALASUBRAMANIAN, R. & TEGONI, G. (1970). *Biochim. Biophys. Acta*, **221**, 165–181.
SHIONO, R. (1968). Private communication.
SOBELL, H. M. (1974). *Sci. Amer.* **231**, 82–91.
STEWART, R. F., DAVIDSON, E. R. & SIMPSON, W. T. (1965). *J. Chem. Phys.* **42**, 3175–3187.
WILSON, A. J. C. (1942). *Nature, Lond.* **150**, 151–152.

Acta Cryst. (1976). B**32**, 3270

Anorthite Quenched from 1530 °C. I. Structure Refinement

BY E. BRUNO, G. CHIARI AND A. FACCHINELLI

Istituto di Mineralogia, Cristallografia e Geochimica dell'Università di Torino, Via San Massimo 24, I-10123 *Torino, Italy*

(*Received* 5 *May* 1976; *accepted* 11 *June* 1976)

Anorthite ($CaAl_2Si_2O_8$) quenched from 1530°C shows only '*a*' and '*b*' type reflexions ($h+k+l=$ even). Two alternative refinements have been carried out, both in the space group $I\bar{1}$: in the first only the Ca atoms are split and the framework atoms are anisotropically refined ($R=0{\cdot}058$); in the second the T and O atoms of the framework are also split and isotropically refined ($R=0{\cdot}062$). On the basis of crystallochemical considerations the split model is assumed to be a better approximation to reality. Among all the possible configurations compatible with the split model, one was chosen on the basis of both crystallochemical considerations and a postulated analogy with low-temperature primitive anorthite. The resulting space group is $P\bar{1}$ which is not supported by the diffractometric evidence (absence of '*c*' and '*d*' reflexions with $h+k+l=$ odd). This absence can be ascribed to the existence of '*c*' antiphase domains small enough to render undetectable the '*c*' and '*d*' reflexions. The quenchability of such '*c*' microdomains may be due to (or favoured by) an imperfect Al–Si alternation induced in the framework by the severe heating. The values of Al occupancies of the T sites indicate a partial Al–Si disorder. Average Al occupancies are $t_1(0)=0{\cdot}56$, $t_1(m)=0{\cdot}46$, $t_2(0)=0{\cdot}51$, $t_2(m)=0{\cdot}47$.

Introduction

The structure of primitive anorthite at room temperature has been solved (Kempster, Megaw & Radoslovich, 1962; Megaw, Kempster & Radoslovich, 1962) and its structural features are now well established. However, there is no general agreement on the significance of the structural variations that take place with thermal treatment, although much research has been done in recent years. All the papers published on this subject report the following diffractometric data: (*a*) the '*a*' reflexions ($h+k=$ even, $l=$ even) remain sharp to the melting point; (*b*) the '*b*' reflexions ($h+k=$ odd, $l=$ odd) remain sharp almost to the melting point; (*c*) the intensities of '*c*' ($h+k=$ even, $l=$ odd) and '*d*' reflexions ($h+k=$ odd, $l=$ even) decrease abruptly with temperature increase and are nearly zero above 230°C (Laves, Czank & Schulz, 1970). This fact can be interpreted either as a systematic extinction or as a decrease in intensity below the detection threshold.

The structures of anorthite refined at high temperature by Czank (1973) [Smith (1974) reports the main

results of the refinement carried out by Czank with intensities collected at 240 and 1430°C] and Foit & Peacor (1973) are relevant to the understanding of the structural modifications that take place when anorthite undergoes heating. Their conclusions, however, are different. Czank (1973) and Czank, van Landuyt, Schulz, Laves & Amelinckx (1973), also on the basis of electron microscopy, suggest a model for temperatures greater than 230°C consisting of a body-centred ($I\bar{1}$) Al–Si framework, while the Ca cations occupy one of the two possible 'split positions' in the large interstices of the framework. The distribution of Ca between the two split positions leads to microdomains $P\bar{1}$, within a matrix $I\bar{1}$. In these microdomains, *i.e.* in some portions of the body-centred framework, the Ca atoms are in primitive ordered arrangement. In the other parts ($I\bar{1}$ matrix) the Ca atoms are either also in a body-centred or in a disordered arrangement. Obviously in such a model the Al–Si framework would no longer contribute to the intensities of '*c*' reflexions.

On the other hand, Foit & Peacor (1973), with data collected at 410 and 830°C, propose a model based on primitive unit cells ($P\bar{1}$) both for the framework and the Ca atoms. They interpret the absence of '*c*' reflexions as a variation of the domain texture (*i.e.* formation of antiphase domains). In contrast to Czank's conclusions, they point out that in the temperature range 25–400°C the experimental data 'do suggest that atomic position and thermal changes within the existing domain structure are not adequate to explain the observed changes in the '*c*' reflexion intensities'.

Let us now consider the reversibility of the modifications induced by heating the sample at different temperatures and then cooling it. (1) For modest temperatures (up to 500°C) the '*c*' domains are not affected, and remain unchanged both in size and shape (Müller & Wenk, 1973). The '*c*' reflexions do not change either, owing to the correspondence between their intensity and the domain texture (Heuer, Nord, Lally & Christie, 1976). (2) For intermediate temperatures (600–1000°C) the size of the '*c*' domains becomes much smaller, and '*c*' reflexions are streaked (Heuer *et al.*, 1976). (3) For very high temperatures (near the melting point), after quenching, the '*c*' and '*d*' reflexions are absent or negligible; also the unit-cell parameters show notable modifications (Kroll, 1971; Smith, 1972; Bruno & Facchinelli, 1974*b*). The variations of γ and γ-related parameters, which in all the feldspars are related to the Al–Si configuration (Ribbe, Stewart & Phillips, 1970; Bruno & Facchinelli, 1974*a*), could indicate that a modification of the Al–Si distribution occurs in the framework at temperatures near the melting point.

Table 1. *Unit-cell parameters*

	Untreated	Quenched from 1530°C
a (Å)	8·173 (1)	8·186 (1)
b (Å)	12·869 (2)	12·876 (2)
c (Å)	14·165 (2)	14·182 (2)
α (°)	93·11 (2)	93·30 (2)
β (°)	115·91 (1)	115·79 (1)
γ (°)	91·26 (1)	91·12 (1)
U (Å^3)	1337·7	1342·2
$\Delta 2\theta^*_{(132-1\bar{3}2)}$	2·30°	2·25°

* Cu $K\alpha$ radiation.

Table 2. *Atomic fractional coordinates* ($\times 10^4$) *and anisotropic thermal parameters* ($\times 10^4$) *in the non-split model*

	x	y	z	β_{11}	β_{22}	β_{33}	β_{12}	β_{13}	β_{23}	B (Å^2)
Ca(000)	2661 (4)	9901 (5)	824 (4)	40 (4)	101 (5)	46 (3)	−19 (3)	16 (3)	−52 (3)	3·26
Ca(0*i*0)	7755 (3)	5369 (2)	5424 (2)	23 (3)	11 (1)	8 (1)	4 (1)	5 (1)	2 (1)	0·58
Ca(*z*00)	2712 (7)	317 (4)	5443 (3)	27 (4)	17 (2)	10 (2)	7 (2)	8 (2)	−1 (2)	0·78
Ca(*zi*0)	7633 (8)	5092 (7)	5699 (5)	32 (5)	91 (7)	44 (4)	−8 (5)	13 (4)	−49 (4)	3·18
T_1(0000)	73 (2)	1587 (1)	1046 (1)	28 (2)	13 (1)	8 (1)	−2 (1)	5 (1)	−1 (1)	0·67
T_1(0*z*00)	31 (2)	1638 (1)	6115 (1)	28 (2)	10 (1)	8 (1)	−3 (1)	4 (1)	−1 (1)	0·60
T_1(*m*000)	9999 (2)	8149 (1)	1194 (1)	35 (2)	10 (1)	7 (1)	3 (1)	7 (1)	1 (1)	0·61
T_1(*mz*00)	37 (2)	8168 (1)	6126 (1)	29 (2)	12 (1)	7 (1)	4 (1)	5 (1)	1 (1)	0·63
T_2(0000)	6872 (2)	1121 (1)	1594 (1)	22 (2)	10 (1)	13 (1)	−1 (1)	2 (1)	−2 (1)	0·66
T_2(0*z*00)	6775 (2)	1059 (1)	6577 (1)	25 (2)	11 (1)	16 (1)	0 (1)	5 (1)	−2 (1)	0·76
T_2(*m*000)	6764 (2)	8814 (1)	1808 (1)	24 (2)	10 (1)	14 (1)	2 (1)	3 (1)	0 (1)	0·70
T_2(*mz*00)	6831 (2)	8758 (1)	6780 (1)	23 (2)	10 (1)	11 (1)	2 (1)	5 (1)	1 (1)	0·62
O_A(1000)	87 (7)	1262 (4)	9908 (4)	103 (9)	25 (3)	11 (2)	10 (4)	21 (4)	0 (2)	1·55
O_A(1*z*00)	6 (7)	1264 (4)	4899 (4)	107 (9)	22 (3)	11 (2)	10 (4)	21 (4)	1 (2)	1·51
O_A(2000)	5744 (5)	9895 (3)	1391 (4)	25 (5)	12 (2)	18 (2)	3 (3)	4 (3)	2 (2)	0·83
O_A(2*z*00)	5729 (6)	9909 (4)	6379 (4)	24 (6)	15 (2)	18 (2)	−1 (3)	2 (3)	−1 (2)	0·90
O_B(0000)	8200 (6)	1001 (4)	913 (4)	52 (7)	16 (2)	32 (3)	−9 (3)	25 (4)	−4 (2)	1·41
O_B(0*z*00)	7994 (6)	1013 (4)	5918 (4)	60 (7)	15 (2)	36 (3)	−7 (3)	32 (4)	−3 (3)	1·55
O_B(*m*000)	8072 (7)	8573 (4)	1241 (5)	60 (8)	20 (3)	58 (4)	−1 (3)	39 (5)	−8 (3)	2·11
O_B(*mz*00)	8216 (7)	8563 (4)	6163 (5)	68 (8)	21 (3)	49 (4)	8 (4)	38 (5)	1 (3)	2·01
O_C(0000)	137 (6)	2797 (4)	1374 (4)	56 (7)	16 (3)	18 (3)	−4 (3)	12 (3)	0 (2)	1·16
O_C(0*z*00)	165 (6)	2929 (4)	6488 (4)	52 (7)	15 (2)	20 (3)	−6 (3)	8 (3)	−4 (2)	1·13
O_C(*m*000)	72 (6)	6807 (4)	1071 (4)	47 (6)	15 (2)	16 (2)	8 (3)	1 (3)	−4 (2)	1·02
O_C(*mz*00)	56 (6)	6904 (4)	6001 (4)	58 (7)	13 (2)	14 (2)	8 (3)	3 (3)	0 (2)	1·00
O_D(0000)	1914 (6)	1041 (4)	1867 (4)	59 (7)	24 (3)	14 (2)	15 (3)	−5 (3)	1 (2)	1·27
O_D(0*z*00)	2005 (7)	1012 (4)	6923 (4)	61 (7)	21 (3)	15 (2)	8 (3)	−13 (3)	−2 (2)	1·23
O_D(*m*000)	1948 (7)	8658 (4)	2200 (4)	64 (8)	25 (3)	26 (3)	5 (4)	−14 (4)	−10 (3)	1·56
O_D(*mz*00)	1855 (8)	8601 (5)	7102 (4)	86 (9)	26 (3)	22 (3)	7 (4)	−17 (4)	−4 (3)	1·69

A structural study of a sample heated near the melting point and quenched could give new data relevant to the problem of the thermal behaviour of anorthite and in particular to the interpretation of high-temperature quenchable transformations. Therefore we decided to elucidate the structure of an anorthite quenched from 1530°C.

Experimental procedure

The sample of anorthite examined was taken from a calc-silicate hornfels from Vesuvius (No. 9332 of the Mineralogical Museum of Turin University catalogue). The crystals are well formed and transparent. The composition of the anorthite was determined from the refractive index of the glass obtained by melting ($1{\cdot}576 > n \gg 1{\cdot}572$) and is An_{100} within the accuracy of the method. This determination was confirmed by the cell dimensions and the $\Delta 2\theta_{(132-1\bar{3}2)}$ obtained from a powder spectrum (Table 1). Weissenberg and precession photographs of a single crystal, before the thermal treatment, show sharp '*a*', '*b*', '*c*' and '*d*' reflexions. A small amount of the sample was heated for about 30 min at 1530°C, then quenched in air to room temperature. After quenching no evidence of melting was detected. The cell dimensions of the quenched material were obtained by least squares from 52 *0* values of unambiguously indexed reflexions measured on a powder spectrum obtained with a Guinier camera (internal-standard correction was applied) (Table 1).

An untwinned fragment was chosen and tested with long-exposure precession and Weissenberg photographs. It showed sharp '*a*' and '*b*' reflexions, while '*c*' and '*d*' were absent. The lack of '*c*' and '*d*' reflexions, if interpreted as systematic extinction, corresponds to a body-centred lattice. Two space groups are possible: $I1$ and $I\bar{1}$. Although the test on the statistical distribution of the normalized structure factors was not discriminating, the centrosymmetric space group was chosen because primitive anorthite has been proved to be centrosymmetric and the loss of a centre of symmetry as a result of a temperature increase seems improbable. Furthermore, all the feldspars with known structure have been considered centrosymmetric. The space group for our quenched anorthite (hereafter AnQ) is then $I\bar{1}$.

The intensities were collected, on the same crystal used for the previous photographs, at the Mineralogical Institute of Perugia University. A Philips PW1100 four-circle diffractometer with graphite-monochromatized Mo radiation and the θ–2θ scan procedure was used. Both '*a*' and '*b*' reflexions were kept on the same scale. There were 2168 '*a*' and 1619 '*b*' reflexions whose intensity exceeded 3σ. The absence of '*c*' and '*d*' reflexions was also confirmed with the diffractometer by measuring a few reflexions, the most intense among those listed by Foit & Peacor (1973). The measured intensities did not exceed background. Intensities were reduced in the conventional manner, although no absorption correction was applied. The crystal dimensions are $0{\cdot}10 \times 0{\cdot}15 \times 0{\cdot}25$ mm.

Refinement of the non-split model

The bytownite (An_{80}) structure (Fleet, Chandrasekhar & Megaw, 1966) was chosen as the starting structure from among the possible ones described in the literature, owing to the common absence of '*c*' and '*d*' reflexions. To match the $I\bar{1}$ space group of AnQ, the 'average structure' ($I\bar{1}$) of bytownite was used. The refinement was carried out with a modified version of the *ORFLS* program (Busing, Martin & Levy, 1962) with the full-matrix approach. The scattering factors were taken from *International Tables for X-ray Crystallography* (1968). A few cycles with individual isotropic temperature factors led to an R of 0·20. R dropped to 0·14 with anisotropic temperature factors for Ca atoms only, and to 0·127 for all atoms. Electron density and difference maps calculated at this stage indicated two distinct positions for each single Ca atom, in analogy with that found by Fleet *et al.* (1966) for bytownite.

Each Ca atom was then substituted by two half-atoms whose coordinates were deduced from the Fourier syntheses. A few more cycles were run, and, on the assumption that the more intense reflexions were affected by secondary extinction, a correction was applied (Stout & Jensen, 1968) (resulting secondary extinction coefficient $g = 2{\cdot}7 \times 10^{-6}$). The final R was 0·058.*

The four Ca half-atoms have been transformed into whole atoms obeying $P\bar{1}$ symmetry, giving a Ca configuration analogous to primitive anorthite. Therefore the body-centring vector becomes a pseudosymmetry element, as for the Ca atoms.

Table 2 shows the coordinates and the temperature factors; Table 3 the root-mean-square displacements of the thermal ellipsoids; Tables 4, 5, 6 and 7 the Ca–O and T–O distances, the O–T–O and T–O–T angles; Table 8 the values of Al occupancy for the various sites. The estimated standard error for all T–O and Ca–O lengths is 0·005 Å, and for O–T–O and T–O–T angles 0·3°.

Refinement of the split model

This model looks satisfactory from a mathematical point of view and agrees with the model proposed by Czank (1973) for anorthite at temperatures higher than 230°C. Nevertheless some doubts remain about its crystallochemical reliability: we do not think that the Ca atoms can occupy one or the other of the two split positions without influencing the position of the other

* A list of structure factors has been deposited with the British Library Lending Division as Supplementary Publication No. SUP 31953 (27 pp., 1 microfiche). Copies may be obtained through The Executive Secretary, International Union of Crystallography, 13 White Friars, Chester CH1 1NZ, England.

Table 3. *Root-mean-square displacements* ($\times 10^3$ Å)

	x	*y*	*z*
Ca(000)	94	119	345
Ca(0*i*0)	74	83	100
Ca(*z*00)	72	90	128
Ca(*zi*0)	92	101	335
T_1(0000)	78	96	108
T_1(0*z*00)	75	89	102
T_1(*m*000)	73	88	101
T_1(*mz*00)	75	86	108
T_2(0000)	72	93	121
T_2(0*z*00)	82	90	128
T_2(*m*000)	79	91	121
T_2(*mz*00)	79	90	101
O_A(1000)	83	141	173
O_A(1*z*00)	84	133	176
O_A(2000)	80	102	132
O_A(2*z*00)	79	113	140
O_B(0000)	92	122	168
O_B(0*z*00)	94	116	178
O_B(*m*000)	103	123	225
O_B(*mz*00)	105	139	201
O_C(0000)	109	124	134
O_C(0*z*00)	92	131	145
O_C(*m*000)	95	98	162
O_C(*mz*00)	95	102	152
O_D(0000)	81	132	182
O_D(0*z*00)	76	127	196
O_D(*m*000)	87	136	225
O_D(*mz*00)	93	145	232

atoms, in particular the more strongly coordinated O atoms. In other words, we do not think it is realistic to postulate a split model for the Ca atoms and a non-split model for the rest of the structure. This opinion is supported by the presence of some anomalous features in the Ca coordination. In particular Table 5 shows that for both Ca(0*i*0) and Ca(*zi*0) the first neighbour O atom is not $O_A(2)$ but $O_A(1)$ and $O_D(0)$ respectively; which would represent an exception among all feldspars. This 'irregular' coordination does not correspond to an actual structural peculiarity of AnQ, but instead is due the unrealistic non-split model. This can be proved by considering that the distances between the Ca atoms and the 'average' O atoms in primitive anorthite (Wainwright & Starkey, 1971) exhibit the same anomalous trend. On the other hand, the thermal ellipsoids of Al, Si and O atoms are very elongated (Table 4) and could hide the presence of two distinct half-atoms in split positions. [See the discussion by H. D. Megaw in the Appendix of Ribbe, Megaw, Taylor, Ferguson & Traill (1969).] Therefore we decided to refine a completely split model. Unfortunately the electron density map around the O and T atoms did not point unambiguously to distinct split positions, unlike the Ca atoms. This probably means that the split lengths for the

Table 4. Ca–O *interatomic distances* (Å)

Ca(000)			Ca(0*i*0)			Ca(*z*00)			Ca(*zi*0)		
O_A(1000)	2·688		O_A(10*i*0)	2·331		O_A(1*z*00)	2·391		O_A(1*zi*0)	2·527	
O_A(100*c*)	2·457		O_A(10*ic*)	2·964		O_A(1*z*0*c*)	2·845		O_A(1*zic*)	2·553	
O_A(2000)	2·291		O_A(20*i*0)	2·339		O_A(2*z*00)	2·328		O_A(2*zi*0)	2·310	
O_A(2*z*0*c*)		3·587	O_A(2*zic*)		>4	O_A(200*c*)		>4	O_A(20*ic*)		3·744
O_A(200*c*)		3·910	O_A(20*ic*)		3·305	O_A(2*z*0*c*)		3·344	O_A(2*zic*)		3·730
O_B(000*c*)	2·457		O_B(00*ic*)	2·364		O_B(0*z*0*c*)	2·366		O_B(0*zic*)	2·473	
O_B(*m*00*c*)		3·460	O_B(*m*0*ic*)	2·628		O_B(*mz*0*c*)	2·599		O_B(*mzic*)		3·070
O_C(0*zi*0)		3·215	O_C(0*z*00)		3·773	O_C(00*i*0)		3·831	O_C(0000)		3·565
O_C(*mzi*0)		3·139	O_C(*mz*00)	2·540		O_C(*m*0*i*0)	2·523		O_C(*m*000)	2·813	
O_D(0000)	2·300		O_D(00*i*0)	2·541		O_D(0*z*00)	2·531		O_D(0*zi*0)	2·290	
O_D(*m*000)	2·833		O_D(*m*0*i*0)		3·696	O_D(*mz*00)		3·589	O_D(*mzi*0)		3·089

Table 5. T–O *bonds* (Å)

T_1(0000)–O_A(1000)	1·649	T_1(*m*000)–O_A(1000)	1·751	T_2(0000)–O_A(2000)	1·757	T_2(*m*000)–O_A(2000)	1·642
O_B(0000)	1·625	O_B(*m*000)	1·707	O_B(0000)	1·744	O_B(*m*000)	1·619
O_C(0000)	1·593	O_C(*m*000)	1·732	O_C(*mz*00)	1·732	O_C(0*z*00)	1·607
O_D(0000)	1·651	O_D(*m*000)	1·697	O_D(*mz*00)	1·693	O_D(0*z*00)	1·634
Mean	1·630	Mean	1·722	Mean	1·732	Mean	1·626
T_1(0*z*00)–O_A(1*z*00)	1·754	T_1(*mz*00)–O_A(1*z*00)	1·652	T_2(0*z*00)–O_A(2*z*00)	1·643	T_2(*mz*00)–O_A(2*z*00)	1·742
O_B(0*z*00)	1·739	O_B(*mz*00)	1·605	O_B(0*z*00)	1·637	O_B(*mz*00)	1·722
O_C(0*z*00)	1·703	O_C(*mz*00)	1·629	O_C(*m*000)	1·627	O_C(0000)	1·715
O_D(0*z*00)	1·766	O_D(*mz*00)	1·590	O_D(*m*000)	1·602	O_D(0000)	1·739
Mean	1·740	Mean	1·619	Mean	1·627	Mean	1·730

Table 6. *Bond angles at* T (°)

	O_A–O_B	O_A–O_C	O_A–O_D	O_B–O_C	O_B–O_D	O_C–O_D
T_1(0000)	102·0	117·4	101·5	111·4	113·2	110·9
T_1(0*z*00)	98·5	119·0	98·0	113·1	115·0	111·8
T_1(*m*000)	101·2	112·4	104·5	114·2	113·9	109·9
T_1(*mz*00)	101·6	113·1	106·1	112·8	114·0	109·0
T_2(0000)	105·0	101·1	109·1	112·7	112·2	115·6
T_2(0*z*00)	106·9	101·6	111·3	112·1	110·3	114·1
T_2(*m*000)	108·6	105·7	108·3	112·0	109·4	112·7
T_2(*mz*00)	108·1	105·5	105·5	110·9	111·5	114·9

framework atoms are rather small; consequently the variance–covariance matrix correlations between half-atoms of the same pair should be large, and the least-squares procedure approaches the limits of significance. Aware of this fact, we tried to refine the split model starting with a trial structure as correct as possible. To accomplish this we have substituted each anisotropic atom with a pair of half-atoms whose positions were calculated from the dimensions and orientation of the thermal ellipsoids in the non-split-model. The orientation of the junction of the two split atoms was assumed to coincide with the direction of the longest axis of the ellipsoid. To calculate the distance of the two split positions we followed an empirical method based on the analogy of AnQ with the structure of primitive anorthite (Wainwright & Starkey, 1971) (AnWS hereafter). The different steps are: (1) we calculated F_c for about 3800 '*a*' and '*b*' reflexions with the coordinates of AnWS and isotropic temperature factors equal for each kind of atom (Al, Si = 0·6; O = 0·7); (2) we applied the body-centring vector to all the Al, Si and O atoms of AnWS, obtaining atom pairs occupying very close positions. Giving an occupancy of $\frac{1}{2}$ to all those atoms we obtained a body-centred split-model equivalent (as far as the F_c's of '*a*' and '*b*' reflexions are concerned) to the model of AnWS; (3) the average positions were calculated for each pair of split atoms and the thermal ellipsoids of these atoms were refined using as F_o data, the F_c calculated in (1). An R of 0·017 after two cycles further demonstrated the substantial equivalence of the isotropic split model and the anisotropic non-split

Table 7. *Bond angles at* O (°)

	O_A		O_B	O_C	O_D
1000	139·5	0000	133·6	132·5	131·1
1*z*00	137·8	0*z*00	133·0	132·0	129·1
2000	124·4	*m*000	154·2	130·2	152·3
2*z*00	124·3	*mz*00	152·4	128·1	151·9

Table 8. *Aluminium occupancy* (t) *of the tetrahedral sites*

t values were calculated from Al/(Al + Si) = 6·58 × [⟨T–O⟩ − 1·605] (Ribbe & Gibbs, 1969).

$t_1(0000) = 0{\cdot}16$	$t_1(m000) = 0{\cdot}77$	$t_2(0000) = 0{\cdot}84$	$t_2(m000) = 0{\cdot}14$
$t_1(0z00) = 0{\cdot}89$	$t_1(mz00) = 0{\cdot}09$	$t_2(0z00) = 0{\cdot}14$	$t_2(mz00) = 0{\cdot}82$
$\langle t_1(0)\rangle = 0{\cdot}53$	$\langle t_1(m)\rangle = 0{\cdot}43$	$\langle t_2(0)\rangle = 0{\cdot}49$	$\langle t_2(m)\rangle = 0{\cdot}48$

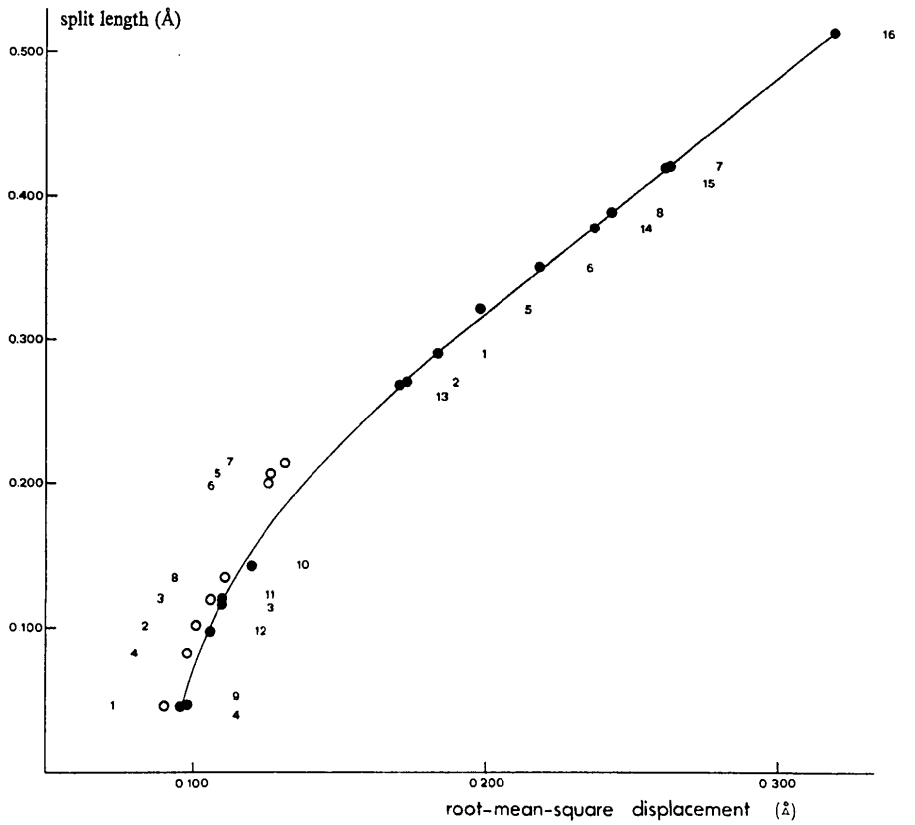

Fig. 1. Split lengths of O and T atoms in AnWS plotted *vs* the r.m.s. displacements of the longest axis of the corresponding thermal ellipsoids in the anisotropic non-split model (see text). Filled circles represent O atoms; open circles Al and Si atoms. The numeration follows the succession of O and T atoms in Table 2.

Table 9. *Atomic fractional coordinates* ($\times 10^4$), *anisotropic thermal parameters* ($\times 10^4$) *of* Ca *atoms and isotropic thermal parameters of* Si, Al *and* O *atoms in the* $P\bar{1}$ *model*

	x	y	z	β_{11}	β_{22}	β_{33}	β_{12}	β_{13}	β_{23}	B (Å^2)
Ca(000)	2662 (4)	9901 (5)	825 (4)	39 (4)	101 (4)	45 (3)	−19 (3)	16 (3)	−51 (3)	3·46
Ca(0*i*0)	7755 (3)	5368 (2)	5424 (2)	23 (3)	11 (1)	7 (1)	4 (1)	4 (1)	2 (1)	0·58
Ca(*z*00)	2709 (6)	316 (4)	5441 (3)	27 (4)	17 (2)	9 (2)	7 (2)	7 (2)	−1 (1)	0·78
Ca(*zi*0)	7635 (7)	5092 (6)	700 (5)	31 (5)	91 (6)	43 (4)	−5 (5)	11 (4)	−49 (4)	3·14

	x	y	z	B (Å^2)		x	y	z	B (Å^2)
T_1(0000)	106 (9)	1548 (5)	1048 (6)	0·29 (14)	O_B(0000)	8121 (17)	1031 (11)	815 (10)	1·11 (22)
T_1(00*i*0)	5033 (10)	6636 (6)	6043 (6)	0·87 (15)	O_B(00*i*0)	3272 (18)	5973 (12)	6002 (11)	0·76 (23)
T_1(0*z*00)	82 (12)	1610 (7)	6111 (7)	0·19 (16)	O_B(0*z*00)	8091 (17)	992 (11)	6020 (10)	0·86 (21)
T_1(0*zi*0)	4970 (12)	6673 (7)	1119 (7)	0·84 (18)	O_B(0*zi*0)	2898 (16)	6036 (10)	816 (9)	0·89 (19)
T_1(*m*000)	9928 (13)	8127 (8)	1187 (9)	0·50 (19)	O_B(*m*000)	8170 (16)	8535 (10)	1395 (10)	1·60 (19)
T_1(*m*0*i*0)	5071 (12)	3172 (7)	6202 (8)	0·52 (18)	O_B(*m*0*i*0)	3000 (13)	3600 (9)	6130 (9)	0·57 (15)
T_1(*mz*00)	79 (8)	8213 (5)	6122 (6)	0·38 (14)	O_B(*mz*00)	8124 (16)	8552 (10)	6058 (10)	0·86 (18)
T_1(*mzi*0)	4991 (9)	3119 (6)	1132 (6)	0·66 (15)	O_B(*mzi*0)	3328 (17)	3577 (11)	1288 (10)	1·47 (20)
T_2(0000)	6896 (10)	1135 (7)	1544 (6)	0·53 (16)	O_C(0000)	186 (37)	2772 (24)	1410 (20)	1·82 (55)
T_2(00*i*0)	1847 (10)	6107 (7)	6644 (6)	0·54 (16)	O_C(00*i*0)	5102 (37)	7817 (24)	6352 (20)	0·46 (53)
T_2(0*z*00)	6768 (8)	1032 (5)	6639 (5)	0·77 (13)	O_C(0*z*00)	202 (23)	2941 (17)	6431 (14)	1·46 (35)
T_2(0*zi*0)	1781 (7)	6082 (5)	1523 (5)	0·40 (12)	O_C(0*zi*0)	5135 (22)	7920 (16)	1531 (13)	0·54 (32)
T_2(*m*000)	6742 (8)	8810 (6)	1863 (5)	0·77 (14)	O_C(*m*000)	9994 (17)	6761 (11)	1119 (11)	0·80 (22)
T_2(*m*0*i*0)	1782 (8)	3819 (6)	6760 (5)	0·37 (13)	O_C(*m*0*i*0)	5148 (17)	1850 (11)	6024 (10)	0·66 (21)
T_2(*mz*00)	6833 (14)	8742 (9)	6746 (8)	0·37 (21)	O_C(*mz*00)	160 (19)	6932 (11)	5973 (11)	0·85 (23)
T_2(*mzi*0)	1828 (14)	3774 (9)	1817 (8)	0·73 (21)	O_C(*mzi*0)	4959 (18)	1878 (11)	1026 (11)	0·68 (23)
O_A(1000)	281 (18)	1302 (11)	9944 (11)	1·67 (22)	O_D(0000)	1785 (17)	973 (11)	1914 (11)	1·71 (22)
O_A(10*i*0)	4963 (17)	6236 (10)	4887 (10)	0·43 (18)	O_D(00*i*0)	6993 (15)	6086 (10)	6836 (10)	0·37 (18)
O_A(1*z*00)	9864 (17)	1243 (9)	4874 (10)	0·54 (18)	O_D(0*z*00)	2105 (15)	1033 (9)	6873 (9)	0·58 (17)
O_A(1*zi*0)	5201 (18)	6295 (10)	9933 (11)	1·45 (21)	O_D(0*zi*0)	6874 (16)	5986 (10)	1984 (9)	1·21 (18)
O_A(2000)	5758 (20)	9880 (14)	1322 (12)	1·01 (28)	O_D(*m*000)	2035 (13)	8700 (9)	2131 (9)	0·69 (15)
O_A(20*i*0)	731 (18)	4906 (13)	6446 (11)	0·30 (23)	O_D(*m*0*i*0)	6831 (15)	3607 (10)	7283 (9)	1·43 (18)
O_A(2*z*00)	5713 (18)	9905 (14)	6435 (12)	0·41 (25)	O_D(*mz*00)	1708 (16)	8575 (10)	7170 (9)	1·44 (17)
O_A(2*zi*0)	751 (20)	4911 (14)	1309 (12)	1·04 (29)	O_D(*mzi*0)	6984 (15)	3623 (9)	2046 (9)	0·93 (16)

Table 10. Ca–O *interatomic distances* (Å)

Ca(000)			Ca(0*i*0)			Ca(*z*00)			Ca(*zi*0)		
O_A(1000)	2·625		O_A(10*i*0)	2·395		O_A(1*z*00)	2·466		O_A(1*zi*0)	2·446	
O_A(100*c*)	2·601		O_A(10*ic*)	2·877		O_A(1*z*0*c*)	2·753		O_A(1*zic*)	2·688	
O_A(2000)	2·318		O_A(20*i*0)	2·339		O_A(2*z*00)	2·331		O_A(2*zi*0)	2·331	
O_A(2*z*0*c*)		3·509	O_A(20*ic*)		3·385	O_A(2*z*0*c*)		3·428	O_A(20*ic*)		3·670
O_A(200*c*)		3·812							O_A(2*zic*)		3·624
O_B(000*c*)	2·368		O_B(00*ic*)	2·417		O_B(0*z*0*c*)	2·436		O_B(0*zic*)	2·392	
O_B(*m*00*c*)		3·653	O_B(*m*0*ic*)	2·487		O_B(*mz*0*c*)	2·499		O_B(*mzic*)		3·192
O_C(0*zi*0)		3·215	O_C(0*z*00)		3·754	O_C(00*i*0)		3·793	O_C(0000)		3·614
O_C(*mzi*0)		3·059	O_C(*mz*00)	2·620		O_C(*m*0*i*0)	2·606		O_C(*m*000)	2·719	
O_D(0000)	2·360		O_D(00*i*0)	2·479		O_D(0*z*00)	2·427		O_D(0*zi*0)	2·410	
O_D(*m*000)	2·686		O_D(*m*0*i*0)		3·876	O_D(*mz*00)		3·744	O_D(*mzi*0)	2·961	

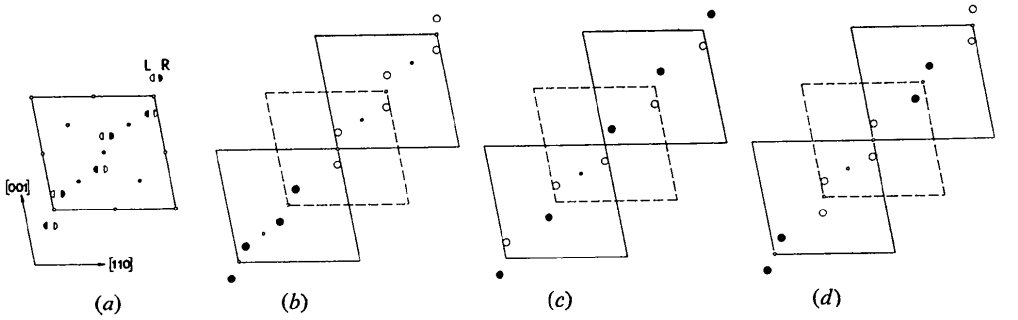

Fig. 2. Alternative atomic configurations of a generic atom in the split model. The models (*b*), (*c*) and (*d*) represent actual structures with whole atoms that can be hidden by the half-atom cell (*a*). Open and filled circles represent atoms in left and right positions respectively. (*a*) $I\bar{1}$ half-atom split model. (*b*) $I\bar{1}$ whole-atom cells. Within each cell an atom occupies only left or only right positions. At the boundary (dashed-lined cell) a $P\bar{1}$ situation occurs. (*c*) $I1$ whole-atom cells. Within each cell an atom occupies both left and right positions. At the boundary a centre of symmetry appears. (*d*) $P\bar{1}$ whole-atom cells. Within each cell an atom occupies both left and right positions. At the boundary an $I\bar{1}$ situation occurs.

model. The longest axis of each thermal ellipsoid of the new model was systematically parallel to the junction of the two split atoms in the starting model (within 3° of approximation);* (4) we plotted the length of the longest axis of the thermal ellipsoids of AnWS (3) *versus* the distance between the two corresponding split positions [AnWS point (2)]. By introducing in this plot (Fig. 1) the dimensions of the longest axis of each ellipsoid of AnQ we obtained, by interpolation, the separation of two corresponding split positions.

In this way we substitute each single anisotropic Al, Si and O atom with a pair of split half-atoms, symmetrically located with respect to the position of the single atom and oriented along the longest axis of the ellipsoid. Two least-squares cycles (with the new coordinates of the split atoms, occupancy $=\frac{1}{2}$, individual isotropic temperature factors for Al, Si and O and the same anisotropic temperature factors obtained in the previous refinement for Ca atoms) led to an R of 0·062.†

Choice of a 'whole-atom' structure

This half-atom split model must hide an actual structure consisting of whole atoms. Many hypotheses are possible, some of which have been discussed in great detail in the literature. A first hypothesis is that the atoms jump from one split position to the other (average in time). This could be rejected on the basis of energetic considerations, in view of the high values of the Ca splits. The other hypotheses are based on a space average and are schematically shown in Fig. 2. In Fig. 2(*a*) the equivalent positions of a generic atom in the half-atom split model ($I\bar{1}$) are drawn. The two split positions are labelled L and R (left and right). If we maintain the cell symmetry $I\bar{1}$, in order to produce the split model as an average effect, we have to postulate two different kinds of cells (Fig. 2*b*), with whole atoms occupying only L positions in the first and only R positions in the second, or *vice versa*. If, on the other hand, both L and R positions occupy the same cell, substitution of one pseudosymmetry element for the corresponding symmetry element would necessarily result. There are two possibilities: the elimination of the centre of symmetry (Fig. 2*c*) or the elimination of the body-centring vector (Fig. 2*d*). In both cases, to obtain the same diffractometric effect of the half-atoms model, it is necessary to postulate the presence of different kinds of cells, obtained from the original ones by the symmetry operation that has been eliminated. It is also necessary that the two kinds of cells of each model are randomly distributed or form microdomains small enough to allow interference of X-rays scattered by neighbour domains, *i.e.* to simulate $I\bar{1}$ symmetry. All three models described above are indistinguishable on the basis of X-ray diffraction evidence. The $I1$ model could be rejected for the same reasons already discussed while choosing the correct space group. The two models $I\bar{1}$ and $P\bar{1}$, tend to be equivalent when the domain dimensions approach those of the unit cell. In fact, at the boundary between two $I\bar{1}$ domains, configurations $P\bar{1}$ occur and *vice versa*, as one can see in Fig. 2. In low-temperature anorthite, $P\bar{1}$ domains, related to one another by an out-of-step vector $\frac{1}{2}[111]$, are present; their dimensions are too large to allow significant X-ray interference. Heating to high temperature causes the domains to become smaller, producing increasingly weak and diffuse '*c*' reflexions. It is acceptable, in agreement with other authors (Foit & Peacor, 1973), that a

* The examination of the AnQ thermal ellipsoids further justifies this substitution for the following reasons: (*a*) many T and O atoms display a strong anisotropy (Table 3); in particular the largest root-mean-square displacements (r.m.s.) on the O atoms in AnQ (O_B and O_D) correspond to the largest splits in AnWS of point (2) [that means to the largest r.m.s. in the anisotropic AnWS non-split model of point (3)]; (*b*) the orientation of the longest axis of the AnQ thermal ellipsoids is rather close (within 20°) to the junction between the two half-atoms of the pair in the AnWS split model obtained at point (2).

† See footnote p. 3272.

Table 11. T–O *bonds* (Å)

$T_1(0000)-O_A(1000)$	1·647	$T_1(m000)-O_A(1000)$	1·745	$T_2(0000)-O_A(2000)$	1·790	$T_2(m000)-O_A(2000)$	1·662
$O_B(0000)$	1·631	$O_B(m000)$	1·678	$O_B(0000)$	1·727	$O_B(m000)$	1·611
$O_C(0000)$	1·620	$O_C(m000)$	1·758	$O_C(mzi0)$	1·759	$O_C(0zi0)$	1·614
$O_D(0000)$	1·619	$O_D(m000)$	1·771	$O_D(mz00)$	1·692	$O_D(0z00)$	1·620
Mean	1·629	Mean	1·738	Mean	1·742	Mean	1·627
$T_1(00i0)-O_A(10i0)$	1·667	$T_1(m0i0)-O_A(10i0)$	1·750	$T_2(00i0)-O_A(20i0)$	1·725	$T_2(m0i0)-O_A(20i0)$	1·639
$O_B(00i0)$	1·638	$O_B(m0i0)$	1·755	$O_B(00i0)$	1·770	$O_B(m0i0)$	1·622
$O_C(00i0)$	1·552	$O_C(m0i0)$	1·712	$O_C(mz00)$	1·724	$O_C(0z00)$	1·589
$O_D(00i0)$	1·704	$O_D(m0i0)$	1·640	$O_D(mzi0)$	1·690	$O_D(0zi0)$	1·636
Mean	1·640	Mean	1·714	Mean	1·727	Mean	1·621
$T_1(0z00)-O_A(1z00)$	1·722	$T_1(mz00)-O_A(1z00)$	1·629	$T_2(0z00)-O_A(2z00)$	1·619	$T_2(mz00)-O_A(2z00)$	1·748
$O_B(0z00)$	1·749	$O_B(mz00)$	1·632	$O_B(0z00)$	1·664	$O_B(mz00)$	1·735
$O_C(0z00)$	1·737	$O_C(mz00)$	1·658	$O_C(m0i0)$	1·668	$O_C(00i0)$	1·705
$O_D(0z00)$	1·745	$O_D(mz00)$	1·542	$O_D(m000)$	1·598	$O_D(0000)$	1·748
Mean	1·738	Mean	1·615	Mean	1·637	Mean	1·734
$T_1(0zi0)-O_A(1zi0)$	1·812	$T_1(mzi0)-O_A(1zi0)$	1·675	$T_2(0zi0)-O_A(2zi0)$	1·659	$T_2(mzi0)-O_A(2zi0)$	1·749
$O_B(0zi0)$	1·734	$O_B(mzi0)$	1·590	$O_B(0zi0)$	1·624	$O_B(mzi0)$	1·711
$O_C(0zi0)$	1·659	$O_C(mzi0)$	1·595	$O_C(m000)$	1·615	$O_C(0000)$	1·726
$O_D(0zi0)$	1·797	$O_D(mzi0)$	1·669	$O_D(m0i0)$	1·597	$O_D(00i0)$	1·721
Mean	1·751	Mean	1·633	Mean	1·624	Mean	1·727

Table 12. *Bond angles at* T (°)

	O_A–O_B	O_A–O_C	O_A–O_D	O_B–O_C	O_B–O_D	O_C–O_D
$T_1(0000)$	104·3	115·2	104·5	108·8	113·4	110·5
$T_1(00i0)$	100·8	120·0	98·5	114·6	110·3	111·1
$T_1(0z00)$	98·7	116·1	99·9	112·7	116·2	112·1
$T_1(0zi0)$	99·3	120·4	95·9	115·0	113·0	111·5
$T_1(m000)$	105·1	114·7	101·3	112·2	112·4	110·6
$T_1(m0i0)$	98·2	109·8	111·1	114·8	113·3	109·3
$T_1(mz00)$	102·2	110·2	112·6	111·8	113·6	106·4
$T_1(mzi0)$	100·7	115·3	102·1	114·2	112·0	111·5
$T_2(0000)$	103·9	97·9	111·8	115·8	110·8	115·1
$T_2(00i0)$	105·4	104·6	107·4	108·6	113·0	116·8
$T_2(0z00)$	108·3	105·0	110·1	106·6	110·2	116·2
$T_2(0zi0)$	104·8	98·1	114·7	117·1	108·8	112·9
$T_2(m000)$	106·5	106·4	113·4	112·6	106·7	111·3
$T_2(m0i0)$	111·2	104·7	104·5	110·6	109·1	116·5
$T_2(mz00)$	110·2	103·5	100·0	111·0	111·2	119·7
$T_2(mzi0)$	105·6	107·7	111·6	111·0	109·1	111·6

decrease in the domain size to a microdomain texture at high temperature reduces the intensities of '*c*' reflexions beyond the limit of detection. These considerations led to the choice of the $P\bar{1}$ model (Fig. 2*d*) as the most plausible actual arrangement of atoms in the AnQ structure.

As pointed out by Fleet *et al.* (1966) for bytownite, a model with a $P\bar{1}$ unit cell containing 26 independent atoms leaves open the choice among 2^{25} possible actual configurations. Criteria based exclusively on plausibility of coordination and of bond lengths allow exclusion of many configurations but do not point to a unique solution. However, the analogy between AnQ and primitive anorthite allows a reasonable, if not proved choice.

Table 9 shows the coordinates and temperature factors of this model. Tables 10, 11, 12, 13 and 14 show the bond distances and angles, and the Al occupancies of the T sites. Estimated errors are 0·013 and 0·018 Å for Ca–O and T–O bonds respectively [they are 0·03Å for bonds involving $O_C(0)$ atoms]; the estimated errors for O–T–O and T–O–T angles are about 0·9°.

Table 13. *Bond angles at* O (°)

	O_A		O_B	O_C	O_D
1000	142·2	0000	130·2	134·7	133·2
10*i*0	136·3	00*i*0	135·0	130·9	128·8
1*z*00	138·5	0*z*00	138·9	132·9	126·5
1*zi*0	135·8	0*zi*0	126·6	132·3	132·0
2000	124·9	*m*000	166·1	127·1	143·4
20*i*0	123·3	*m*0*i*0	146·1	131·5	164·7
2*z*00	123·2	*mz*00	145·8	130·8	164·3
2*zi*0	125·0	*mzi*0	159·2	124·7	141·9

Comparison between the two models

For the Ca atoms the two refinements led to identical positional and thermal parameters, within the standard deviations. It has been necessary to split both Ca(000) and Ca(*z*00) into two half-atoms, according to the Fourier map indications of two distinct positions for each single Ca atom. The two structures differ only in the framework: one is described by whole anisotropic atoms and the other by isotropic half-atoms, both with space group $I\bar{1}$. The split model allows one to pass to a whole-atom model, with unit cell $P\bar{1}$, analogous to primitive anorthite. This analogy strongly supports the reliability of the split model.

AnQ shows a certain degree of disorder which has been interpreted in terms of out-of-phase microdomains of $P\bar{1}$ cells, which simulate an overall $I\bar{1}$ symmetry. In the non-split model, this disorder is revealed in the elongation of the thermal ellipsoids, which is larger than predictable for a feldspar structure on the basis of thermal motion alone. The resulting atomic coordinates are the average of the positions actually occupied by the atoms in the single cells or subcells. Under these conditions, the accuracy inferred by the standard deviations calculated by least squares should not be considered real. The errors in the bond distances and angles are actually much larger than those estimated from the e.s.d.'s with the normal procedure. The values of the average Al occupancies of the T sites, obtained from the dimensions of the tetrahedra, are significantly lower than the theoretical value determined on the basis of the experimental chemical composition. This anomalous result could partially be diminished by

Table 14. *Aluminium occupancy* (*t*) *of the tetrahedral sites*

See Table 8 for the definition of *t*.

$t_1(0000)=0{\cdot}16$	$t_1(m000)=0{\cdot}88$	$t_2(0000)=0{\cdot}90$	$t_2(m000)=0{\cdot}14$
$t_1(00i0)=0{\cdot}23$	$t_1(m0i0)=0{\cdot}72$	$t_2(00i0)=0{\cdot}80$	$t_2(m0i0)=0{\cdot}11$
$t_1(0z00)=0{\cdot}88$	$t_1(mz00)=0{\cdot}07$	$t_2(0z00)=0{\cdot}21$	$t_2(mz00)=0{\cdot}85$
$t_1(0zi0)=0{\cdot}96$	$t_1(mzi0)=0{\cdot}18$	$t_2(0zi0)=0{\cdot}12$	$t_2(mzi0)=0{\cdot}80$
$\langle t_1(0)\rangle=0{\cdot}56$	$\langle t_1(m)\rangle=0{\cdot}46$	$\langle t_2(0)\rangle=0{\cdot}51$	$\langle t_2(m)\rangle=0{\cdot}47$

using distances corrected for thermal vibration (which are longer than the uncorrected distances); however, this correction would not help to explain the anomalies of the Ca coordination. (These anomalies for both distances and angles are highly significant, even with the higher estimated errors discussed above.)*

In the split model, the disorder present in the crystal is treated by splitting each atom into a pair of half-atoms. The positions of these half-atoms could be determined by least squares with low accuracy, because of the strong correlations present in the variance–covariance matrix. These correlations also influence the e.s.d.'s, because of the full-matrix refinement. In fact, the e.s.d.'s of the coordinates of the split model are up to three times as large as those obtained for the non-split model. The high value of the e.s.d.'s requires an accurate analysis of the reliability of the results at every step of the discussion. Another possible source of error in the distances and angles is the partially arbitrary choice of one of the 2^{25} possible $P\bar{1}$ configurations; but a quantitative evaluation of this could not be made.

In conclusion, the two models are approximations to physical reality, and the split model, within the accuracy limits discussed above, could be considered more reliable. In the following discussion the distances and angles are those calculated from the $P\bar{1}$ split-model atomic coordinates.

Discussion

A detailed comparison with the structure of AnWS and the discussion of the crystallochemical aspects of the structural modifications induced in anorthite by the thermal treatment, are deferred to a subsequent paper (Chiari, Facchinelli & Bruno, in preparation).

(1) *Thermal parameters*

The thermal parameters (Table 11) show peculiar trends, especially for Ca and O atoms. For the Ca atoms, the isotropic B values (estimated from the anisotropic refinement by averaging the diagonal elements B_{ii} of the matrix describing the anisotropic thermal ellipsoids) are less than 1 in the (z00) and (0i0) sites, and greater than 3 in (000) and (zi0) sites. The latter two high values are a consequence of strongly elongated thermal ellipsoids. A difference between the isotropic B values of each pair of split Ca atoms is also present in AnWS, although not as large as in AnQ. In the anorthite refined at 410 °C by Foit & Peacor (1973) these differences are intermediate between AnWS and AnQ.

The isotropic thermal parameters of most pairs of O atoms in AnQ are markedly different. The oxygen B values are not randomly distributed. In fact, O atoms coordinated by Ca with high thermal parameters [*i.e.* Ca(000) and Ca(zi0)] have, in general, high thermal parameters as well; O atoms coordinated by Ca with low thermal parameters [*i.e.* Ca(0i0) and Ca(z00)] have low values of B. Whereas some of the differences between B values of individual pairs cannot be considered significant, owing to their very high e.s.d.'s, the differences between the average B's of O atoms coordinated by each Ca are highly significant. To calculate these averages only those O atoms within a distance of 3 Å have been considered coordinated by the Ca. The values of the means so obtained are listed in Table 15 for both AnQ and AnWS, together with the individual B's for Ca atoms. In conclusion, the B values of the O atoms seem to depend upon the B values of the coordinating Ca. This correlation could also support the $P\bar{1}$ model chosen from the 2^{25} possible.

Table 15. *Thermal parameters of calcium and* Ca-*bonded oxygens and relevant* Ca–O *distances*

B_{Ca}: isotropic B of Ca atoms; $\langle B_O \rangle$: average isotropic B of Ca-bonded O atoms; $\langle Ca^{VII}\text{–}O \rangle$: average Ca–O bond lengths; r.m.s.d.: root-mean-square displacements along the longest axes of the thermal ellipsoids of Ca atoms.

		Ca(000)		Ca(zi0)	
		AnQ	AnWS	AnQ	AnWS
B_{Ca}	(Å²)	3·46	1·20	3·14	1·43
$\langle B_O \rangle$	(Å²)	1·31	0·70	1·11	0·79
$\langle Ca^{VII}\text{–}O \rangle$	(Å)	2·567	2·547	2·564	2·525
r.m.s.d.	(Å)	0·344	0·176	0·339	0·202
Ca–$O_D(m)$	(Å)	2·686	2·538	2·961	2·717
		Ca(z00)		Ca(0i0)	
		AnQ	AnWS	AnQ	AnWS
B_{Ca}	(Å²)	0·78	0·80	0·58	0·86
$\langle B_O \rangle$	(Å²)	0·64	0·70	0·53	0·71
$\langle Ca^{VII}\text{–}O \rangle$	(Å)	2·503	2·490	2·517	2·503
r.m.s.d.	(Å)	0·128	0·130	0·101	0·132
Ca–$O_B(m)$	(Å)	2·499	2·494	2·487	2·494

The thermal parameters of Ca could be interpreted in terms of Ca coordination. The cation environments in the four non-equivalent sites are slightly different, but the average distances of the first seven neighbours [2·57, 2·56, 2·50 and 2·52Å in (000), (zi0), (z00) and (0i0) respectively] do not differ enough to explain the variation of the Ca thermal parameters. On the other hand, bearing in mind that the high B values are due to a strong anisotropy, it is useful to analyse the trend of those Ca–O bonds whose orientation is close to the direction of the longest axis of the Ca thermal ellipsoid, namely Ca–$O_D(m)$ in the (000) and (zi0) sites and Ca–$O_B(m)$ in the (z00) and (0i0) sites. The four values are 2·69, 2·96, 2·50, 2·49Å respectively (Table 15). They are significantly different in pairs; a correlation between the Ca thermal parameters and the O coordination seems evident. From Table 15 one can also see that some features observed in AnQ are present in AnWS as well. It remains questionable if this is because of an

* Two variables, A and B, affected by e.s.d.'s equal to σ_A and σ_B, are supposed to be significantly different if $A-B>2\sigma$, where $\sigma^2=\sigma_A^2+\sigma_B^2$. When a variable C is the average over N values affected by σ_c, its e.s.d. is $\sigma_n=\sigma_c/\sqrt{N}$.

actual thermal vibration (average in time) or of a statistical distribution over only slightly different positions in the various unit cells (average in space). The values themselves, ($B > 3$) anomalously high, strongly support the latter hypothesis. In both cases it seems likely that the thermal parameters of the O atoms coordinated by Ca are influenced by the latter.

Finally, Czank (1973) [see Smith (1974)] refined the occupancy of the Ca sites, obtaining low values in (000) and ($zi0$) and high values in ($z00$) and ($0i0$) sites. We do not have direct information on the refinement carried out by Czank, so we cannot discuss his results in detail. We can notice, though, a certain correspondence between Czank's high values of occupancy and our low values of B and *vice versa*.

(2) *The* Al *occupancies*

The Al occupancies of the individual T sites allow, as predictable, the main division into Si-rich and Al-rich tetrahedra. Within both groups, the variations of the Al content are slight or not significant when tested with the above-quoted procedure. Averaging these values over the sites related by the pseudosymmetry vectors $\frac{1}{2}[111]$ and $\frac{1}{2}[001]$, four values of the Al occupancy are obtained, corresponding to the four independent sites $T_1(0)$, $T_1(m)$, $T_2(0)$, $T_2(m)$ in an average structure $C\bar{1}$. Differences among these values (Table 14) are significant and the trend shown is well defined: they give evidence of a certain degree of Al–Si disorder and a concentration of Al in the $T_1(0)$ sites.

In a primitive anorthite, a perfect Al–Si succession, as imposed by the Al-avoidance rule (Loewenstein, 1954), leads to mean Al occupancies equal to 0·5 for the above four sites. In AnQ the Al occupancies vary from 0·56 to 0·46, decreasing in the order: $t_1(0)$, $t_2(0)$, $t_2(m)$, $t_1(m)$. A possible explanation of this observation is that the Al–O–Al bonds formed when Al–Si succession is not perfect are less severely forbidden at temperatures close to the melting point than at room temperature. Among all the possible Al–Si exchanges taking place at very high temperature, those increasing the Al-content in $T_1(0)$ sites are favoured. This tendency could be related to the analogous phenomenon of the Al concentration in $T_1(0)$ observed in all triclinic 'ordered' feldspars with a Si/Al ratio > 1. In conclusion, severe thermal treatment would induce in the anorthite framework a certain amount of disorder, *i.e.* an imperfect Al–Si succession; paradoxically, this disorder would favour segregation of Al in the $T_1(0)$ sites. The apparent contradiction of this tendency with respect to the order–disorder phenomena in the alkali feldspars and in the plagioclases will be considered with a quantitative and more detailed discussion of this observation in a subsequent paper.

The Al occupancies, on the other hand, can be related to the absence of 'c' reflexions in AnQ. It is well known that the presence of 'c'-antiphase microdomains (*i.e.* related by a vector $\frac{1}{2}[111]$) can explain the absence of 'c' reflexions in a $P\bar{1}$ structure. The quenchable disappearance of 'c' reflexions is interpreted as due to the formation, during heating, of microdomains which are 'frozen in' during quenching. This hypothesis is consistent with the observations and deductions of Laves & Goldsmith (1955) on the thermal changes in anorthite. On the other hand, the Al occupancy discussed above could lead to a more complex interpretation: an imperfect Al–Si succession somehow inhibits the 'c' domains from growing large enough to allow the 'c' reflexions to have a measurable intensity. This is in agreement with the observations of Goldsmith & Laves (1956). Since this imperfect succession induced at very high temperature is a diffusive quenchable transformation, the absence of 'c' reflexions, when induced at very high temperature, is also quenchable. This hypothesis could explain why the 'c' reflexion intensity variations are not quenchable for moderate but are quenchable for severe heating.

Furthermore, this hypothesis agrees with the absence of 'c' reflexions in those low-temperature plagioclases in which the Si/Al ratio is even just slightly > 1 (see bytownite). In this case a Si/Al ratio > 1 would inhibit a perfect Al–Si succession with the same disorder result induced in the pure anorthite by heating close to the melting point.

We thank P. F. Zanazzi for the use of the PWI-1100 diffractometer at Perugia University and for help during the collection of the intensities. We are grateful to G. Ferraris for helpful suggestions and critical reading of the manuscript.

This work was supported by Consiglio Nazionale delle Richerche, Roma.

References

Bruno, E. & Facchinelli, A. (1974*a*). *Bull. Soc. Fr. Minér. Crist.* **97**, 378–385.

Bruno, E. & Facchinelli, A. (1974*b*). *Bull. Soc. Fr. Minér. Crist.* **97**, 422–432.

Busing, W. R., Martin, K. O. & Levy, H. A. (1962). *ORFLS*. Oak Ridge National Laboratory Report ORNL-TM-305.

Czank, M. (1973). *Strukturen des Anorthits bei höheren Temperaturen*. Thesis, E. T. H., Zürich.

Czank, M., van Landuyt, J., Schulz, H., Laves, F. & Amelinckx, S. (1973). *Z. Kristallogr.* **138**, 403–418.

Fleet, S. G., Chandrasekhar, S. & Megaw, H. D. (1966). *Acta Cryst.* **21**, 782–801.

Foit, F. F. & Peacor, D. R. (1973). *Amer. Min.* **58**, 665–675.

Goldsmith, J. & Laves, F. (1956). *Z. Kristallogr.* **107**, 396–405.

Heuer, A. H., Nord, G. L. Jr, Lally, J. S. & Christie J. .M (1976). *Electron Microscopy in Mineralogy*, edited by H. R. Wenk, pp. 345–353. Berlin: Springer Verlag.

International Tables for X-ray Crystallography (1968). Vol. III, 2nd ed. Birmingham: Kynoch Press.

Kempster, C. J. E., Megaw, H. D. & Radoslovich, E. W. (1962). *Acta Cryst.* **15**, 1005–1017.

KROLL, H. (1971). *Feldspäte im System* $K[AlSi_3O_8]$–$Na[AlSi_3O_8]$–$Ca[Al_2Si_2O_8]$: Al, Si *Verteilung und Gitterparameter, Phasen-Transformationen und Chemismus.* Thesis, Westfälischen Wilhelms-Univ., Münster.
LAVES, F., CZANK, M. & SCHULZ, H. (1970). *Schweiz. miner. petrogr. Mitt.* **50**, 519–525.
LAVES, F. & GOLDSMITH, J. R. (1955). *Z. Kristallogr.* **106**, 227–235.
LOEWENSTEIN, W. (1954). *Amer. Min.* **39**, 92–96.
MEGAW, H. D., KEMPSTER, C. J. E. & RADOSLOVICH, E. W. (1962). *Acta Cryst.* **15**, 1017–1035.
MÜLLER, W. F. & WENK, H. R. (1973). *Neues Jb. Miner. Mh.* pp. 17–26.
RIBBE, P. H. & GIBBS, G. V. (1969). *Amer. Min.* **54**, 85–94.
RIBBE, P. H., MEGAW, H. D., TAYLOR, W. H., FERGUSON, R. B. & TRAILL, R. J. (1969). *Acta Cryst.* B**25**, 1503–1518.
RIBBE, P. H., STEWART, D. B. & PHILLIPS, M. W. (1970). Proc. Geol. Soc. Amer. Meeting, Milwaukee. Abstracts, p. 663.
SMITH, J. V. (1972). *J. Geol.* **80**, 505–525.
SMITH, J. V. (1974). *Feldspar Minerals.* Vol. 1. *Crystal Structure and Physical Properties.* Berlin: Springer Verlag.
STOUT, G. H. & JENSEN, L. H. (1968). *X-ray Structure Determination.* New York: Macmillan.
WAINWRIGHT, J. E. & STARKEY, J. (1971). *Z. Kristallogr.* **133**, 75–84.

Acta Cryst. (1976). B**32**, 3280

A Structure Analysis of the Compound $K_{0\cdot27}WO_{(3+y)}$

BY P. GOODMAN

Division of Chemical Physics, CSIRO, P.O. Box 160, *Clayton, Victoria, Australia* 3168

(*Received* 23 *January* 1976; *accepted* 12 *May* 1976)

The structure of the compound $K_xWO_{(3+y)}$ with $x \simeq 0{\cdot}27$ and $y = x/2$ has been studied by X-ray and electron diffraction. The structure resembles an ordered hexagonal tungsten bronze. Crystals for the structural study were prepared by vapour transport growth and annealed at high temperature. This preparation allowed two types of ordering to be distinguished, one involving the host WO_3 lattice and the other involving the K^+ structure. It was found that the value of y in the above formula can be varied over a certain range without a major structural change; the structural influence of small changes in O content has been studied.

1. Introduction

A study has been made of the crystal structure of the non-stoichiometric compounds $K_xWO_{(3+y)}$, where x is approximately 0·27 and y ranges between the limits of zero and 0·27/2. This study was carried out in three stages: crystal growth, diffraction study, and a study of oxidation. Initially conditions were found for growing crystals of uniform structure in plate and needle morphology by vapour transport. These were required for X-ray and electron diffraction and electron microscopy investigations, and allowed a semi-quantitative structure determination. Finally a study was made of the oxidation and reduction over a range of stoichiometry, within which the process appeared to be completely reversible, and to take place without loss of morphology. For this latter study both the vapour-grown crystals and the more readily available crystals produced by solid-state reaction were used.

A preliminary report (Denne & Goodman, 1973) gave the unit-cell parameters obtained from the vapour-grown crystals. However, at the time of that report the evidence of Deschanvres, Desgardin, Raveau & Thomazeau (1967) had not been noted. These authors studied the oxidation and reduction between the tungsten bronze and the tungstate of similar potassium content to our preparations. After a comparison of the two sets of data (*i.e.* 1967 and 1973) it became evident that our crystals were in a higher state of oxidation than originally stated. It was also evident that the earlier authors were working with twinned crystals and without the aid of electron diffraction, and consequently failed to find the true unit cell and symmetry of the structure. The twinning morphology and identification of the true symmetry was discussed in our 1973 report. It is now possible to give many additional features of the structure as a consequence of electron diffraction and electron microscope analysis, and additional chemical evidence of the type presented by Deschanvres *et al.*

2. An outline of the structure

The ordered structure consists of the addition of two almost totally independent structures, namely the WO_3 lattice which adopts a slightly distorted version of the hexagonal tungsten-bronze structure (Magnéli & Blomberg, 1951), plus a structure of K^+ ions exhibiting long and short-range ordering. After high-temperature annealing in air, long-range ordering of the K^+ ions in the **a*** direction is complete, every fourth interstitial plane being almost completely vacant. K^+ ion sites